A novel application of multivariable 1 adaptive control: From design to real-time implementation on an underwater vehicle

Divine Maalouf, Vincent Creuze, Ahmed Chemori

A Novel Application of Multivariable $\mathcal{L}_1$ Adaptive Control : from Design to Real-Time Implementation on an Underwater Vehicle

Divine Maalouf[1] Vincent Creuze[1] and Ahmed Chemori[1]

***Abstract*— This paper presents the design and experimental implementation of an $\mathcal{L}_1$ adaptive control on a tethered underwater vehicle. This controller, well known for its fast adaptation and its robusntess, is proposed to be applied for the first time in the field of underwater vehicles control. This paper summarizes the implementation and experimental results obtained on a modified version of the AC-ROV underwater vehicle. Various experimental scenarios are presented to illustrate the ability of the $\mathcal{L}_1$adaptive law not only to successfully control pitch and depth (even with strong modeling uncertainties), but also to be efficient towards disturbances like waves or buoyancy changes.**

I. INTRODUCTION

Underwater vehicles have gained an increased interest in the last decades given the multiple of operations they can perform in various fields. We are particularly interested in the category of tethered vehicles also called Remotely Operated Vehicles (ROV). Different challenges in autonomous control of such systems arise from the inherent high nonlinearities and time varying behavior of the vehicle's dynamics subjected to different hydrodynamic effects and disturbances. To solve this problem, various control approaches to solve this control problem can be found in the litterature. $\mathcal{H}_\infty$ control was proposed and tested in simulation [1]. Various chattering free sliding mode schemes have been proposed for such systems to cope with big uncertainties and were experimentally validated [2]. Intelligent control methods applying reinforcement learning or artifical intelligence can be found in [3][4] and [5] where simulation results are provided and an experimental study was reported in [6]. Adaptive control schemes are seen to be very commun in such applications [7][8][9]. The use of an adaptive controller is motivated in particular by the presence of uncertainties in the model parameters and their likelihood to change. The salinity changes the buoyancy parameter; the addition of sensors or the manipulation of objects changes the mass parameters and the damping parameters are greatly affected by the encounter of algae or moving obstacles. For similar reasons, adaptive controllers have been used for system identification and are highly appreciated within the aircaft control community. However, despite their success in many applications, they hold some drawbacks [10]. For instance, in [11] an extensive study has been made to show that a wide range of such controllers has been used with restrictive assumptions and concluded that adaptive controllers exhibit undesirable frequency characteristics. They also rely on the need of a persistancy in parameter excitation before convergence which may lead to a bad transient behavior [12]. Consequently, several attempts have been proposed to overcome the shortcomings of these controllers. A large adaptation gain leads to undesirable effects with the risk of parameter divergence. That's why most of the methods suggest limiting this gain at the cost of a slower adaptation and convergence [13]. The recently developped $\mathcal{L}_1$ adaptive controller [14] eliminates the need of such a tradeoff since it relies on an architecture where robustness and adaptation are decoupled. It is based on the use of a low pass filter in its feedback loop and is only limited by the hardware capabilities since the adaptation gain can be increased as much as needed to achieve a faster convergence given that the boundedness of the parameters' evolution is ensured by the projection operator present in the adaptation law. The proof of asymptotic stability of this controller is performed through the small gain theorem [14]. This control scheme is able to revisit the failures of other adaptive controllers by maintaining its performance and robustness in situations where the other controllers cannot [15][16]. The $\mathcal{L}_1$ adaptive controller has been validated through simulations and experiments mainly on aerial vehicles [17][18], but it was also seen in other applications such as the control of the acrobot [19] and the hysteris in smart materials [20]. The main contribution of this paper is the experimental demonstration of a new application of this controller which concerns depth and pitch control of an underwater vehicle. To the best knowledge of the authors, this method has never been applied yet to control of underwater vehicles. This paper is organized as follows: in the second section we present the dynamic modeling of the system, the third section shows the theoretical aspect of this controller and its novel design for implementation on underwater vehicles. The fourth section presents the prototype and the experimental setup and in the fifth section we analyze the experimental results. The paper ends with some concluding remarks.

II. Dynamic Modeling of the System

By considering the inertial generalized forces, the hydrodynamic effects, the gravity, and buoyancy contributions as well as the effects of the actuators (thrusters), the dynamic model of an underwater vehicle in matrix form, using the SNAME notation and the representation proposed by Fossen [21] is written as:

$$\dot{\eta} = J(\eta)\nu \tag{1}$$

$$M\dot{\nu} + C(\nu)\nu + D(\nu)\nu + g(\eta) = \tau + w_d \tag{2}$$

[1]D. Maalouf, V. Creuze and A. Chemori are with LIRMM, Université Sud de France (UMSF), CNRS, 34095 Montpellier, France vincent.creuze@lirmm.fr

where $\nu = [u, v, w, p, q, r]^T, \eta = [x, y, z, \phi, \vartheta, \psi]^T$ are vectors of velocities (in the body-fixed frame) and position/Euler angles (in the earth-fixed frame) respectively (cf. Fig. 1).
$J(\eta) \in \mathbb{R}^{6\times6}$ is the Jacobian transformation matrix mapping the body-fixed frame to the earth-fixed one. The model matrices M, C, and D denote inertia (including added mass), Coriolis-centripetal (including added mass), and damping respectively, while g is a vector of gravitational/buoyancy forces. τ is the vector of control inputs and w_d the vector of external disturbances. In the case of our study, the vehicle used has a slow dynamics, and hence it will be moving at velocities low enough to make the Coriolis terms negligible ($C(\nu) \approx 0$).

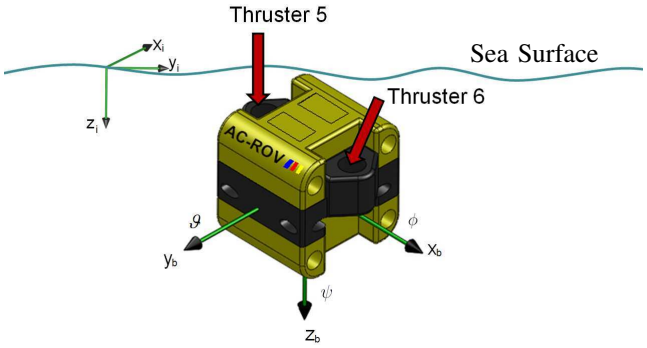

Fig. 1: View of the AC-ROV reference frames ($x_i y_i z_i$: earth-fixed frame, $x_b y_b z_b$: body-fixed frame).

Equation (2) describes the dynamics of the system in six degrees of freedom taking into account the three translations and three orientations. The input vector $\tau \in \mathbb{R}^6$ considers six actions on the system to fully control it. The presented formulation of the robot's dynamics is expressed in the body frame and can be transformed to the earth frame by using the kinematic transformations of the state variables and the model parameters as shown below:

$$\begin{aligned} \dot{\eta} &= J(\eta)\nu \\ \ddot{\eta} &= J(\eta)\dot{\nu} + \dot{J}(\eta)\nu \\ M^*(\eta) &= J^{-T}(\eta)\, M\, J^{-1}(\eta) \\ D^*(\nu,\eta) &= J^{-T}(\eta)\, D(\nu)\, J^{-1}(\eta) \\ g^*(\eta) &= J^{-T}(\eta)\, g(\eta) \\ \tau^* &= J^{-T}(\eta)\, \tau \\ w_d^* &= J^{-T}(\eta)\, w_d \end{aligned} \tag{3}$$

Equation (2) can therefore be expressed in the earth frame as:

$$M^*(\eta)\ddot{\eta} + D^*(\nu,\eta)\dot{\eta} + g^*(\eta) = \tau^* + w_d^* \tag{4}$$

In this paper, we are studying the dynamics of the vehicle in its translational motion along the z axis and its orientation with respect to the pitch angle. Therefore, we will get $M^*(\eta), D^*(\eta) \in \mathbb{R}^{2\times2}$ and $g^*, \tau^*, w_d^* \in \mathbb{R}^2$.
τ^* is the control input expressed in the earth frame in Newton and is given by:

$$\tau^* = J^{-T} T K u \tag{5}$$

where $u \in \mathbb{R}^2$ is the vector of control inputs expressed in volts (as depicted on Fig.1, we have two vertical thrusters acting simultaneously on the two degrees of freedom of interest), K is the force coefficient in Newton.Volt^{-1}. $T \in \mathbb{R}^{2\times2}$ is the actuators' configuration matrix, taking into account the position and orientation of the thrusters.

III. Problem Formulation and Proposed Solution

Our objective is to perform depth and pitch control of a highly nonlinear system with unknown and varying model parameters in presence of disturbances. For this purpose, a robust adaptive controller will be proposed. In this section, the state space representation extracted from the dynamical model (4) will be used for the design of the $\mathcal{L}_1$ adaptive controller implemented for the first time on an underwater vehicle.

A. Problem Formulation

We consider the following class of systems [14]:

$$\begin{aligned} \dot{x}_1(t) &= x_2(t) & x_1(0) &= x_{1_0} \\ \dot{x}_2(t) &= A_2 x_2(t) + f_2(t, x(t)) + B_2 \omega u & x_2(0) &= x_{2_0} \\ y(t) &= C x(t) \end{aligned} \tag{6}$$

where $x_1 \in \mathbb{R}^n$ and $x_2 \in \mathbb{R}^n$ are the states of the system forming the complete state vector: $x(t) = [x_1(t),\ x_2(t)]^T$. A_2 is a known $n \times n$ matrix and $B_2 \in \mathbb{R}^{n\times m}$ is a constant full rank matrix. $u(t) \in \mathbb{R}^m$ is the control input vector ($m \leq n$) and $\omega \in \mathbb{R}^{m\times m}$ is the uncertainty on the input gain. $C \in \mathbb{R}^{m\times n}$ is a known full rank constant matrix, $y \in \mathbb{R}^m$ is the measured output and f_2 is an unknown nonlinear function. In a more compact matrix form, the system (6) becomes:

$$\dot{x} = Ax + f + B_m \omega u \tag{7}$$

with $A = \begin{bmatrix} 0_{n\times n} & \mathbb{I}_n \\ 0_{n\times n} & A_2 \end{bmatrix}$, $f = \begin{bmatrix} 0_{n\times1} \\ f_2 \end{bmatrix}$ and $B_m = \begin{bmatrix} 0_{n\times m} \\ B_2 \end{bmatrix}$
Applying the same formalism as equation (6), the state space representation of the studied dynamics is extracted from the dynamic model (4) and given by:

$$\begin{bmatrix} \dot{\eta}_1 \\ \dot{\eta}_2 \end{bmatrix} = \begin{bmatrix} 0_{2\times2} & \mathbb{I}_2 \\ 0_{2\times2} & \frac{-D^*}{M^*} \end{bmatrix} \begin{bmatrix} \eta_1 \\ \eta_2 \end{bmatrix} - \begin{bmatrix} 0_{2\times1} \\ \frac{g^*}{M^*} - \frac{w_d^*}{M^*} \end{bmatrix} + \begin{bmatrix} 0_{2\times2} \\ \frac{1}{M^*} \end{bmatrix} \omega\tau^* \tag{8}$$

where $\eta_1 = [z,\ \vartheta]^T$ and $\eta_2 = [\dot{z}, \dot{\vartheta}]^T$. τ^* is expressed in Newton and ω is the uncertainty on the input gain. In this case $\omega \in \mathbb{R}^{2\times2}$ is considered to be a diagonal matrix.
The output vector is given by:

$$y = \begin{bmatrix} 1 & 0 & 0 & 0 \\ 0 & 1 & 0 & 0 \end{bmatrix} \begin{bmatrix} \eta_1 \\ \eta_2 \end{bmatrix} = \begin{bmatrix} z \\ \vartheta \end{bmatrix} \tag{9}$$

B. Proposed Solution: $\mathcal{L}_1$ Adaptive Controller

To control the system (8)-(9), an $\mathcal{L}_1$ adaptive controller is proposed. The choice of this controller is motivated by its architecture based on a decoupling between adaptation and robustness. High adaptation gains can be chosen securing a fast convergence with a smooth transient response. This architecture described in [14] is shown in the block diagram of Fig. 2. Block 1 is the studied system extracted from (6) with A_m being a chosen Hurwitz matrix determining the

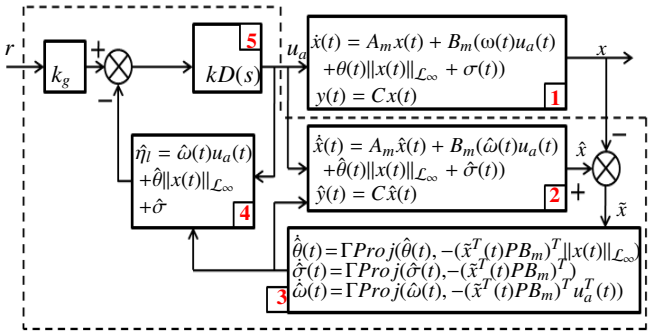

Fig. 2: Block Diagram of the closed-loop $\mathcal{L}_1$ adaptive controller.

desired closed-loop dynamics and calculated using a gain k_m: $A_m = A - B_m k_m$ with A being the state matrix and B_m the input matrix of the open-loop system (8). The unknown linear function f_2 has been decomposed into a parameter state dependent part $\theta(t)\|x(t)\|_{\mathcal{L}_\infty}$, being $\|x(t)\|_{\mathcal{L}_\infty}$ the infinity norm of the state x at time t, and a nonlinear part σ, which accounts for the external disturbances. The $\mathcal{L}_1$ controller's architecture is delimited with dashed lines in Fig. 2. It is composed of 3 main stages. The prediction stage (block 2), where the states of the system as well as the outputs are calculated at every iteration using the parameters' estimation. The adaptation stage (block 3) uses the error $\tilde{x}$ between the measured states and the estimated ones to adapt the parameters using a projection method in order to ensure their boundedness. The parameter P shown in the block 3 is the solution of the algebraic Lyapunov equation: $A_m^T P + PA_m^T = -Q$ for any arbitrary symmetric matrix $Q = Q^T > 0$. Γ is the adaptation gain. The last stage (blocks 4 and 5) pertains to the design and implementation of the control's input filter. $D(s)$ is an $m \times m$ strictly proper transfer function leading to a stable closed-loop filter: $C(s) = \frac{\omega k D(s)}{\mathbb{I}_m + \omega k D(s)}$. k is a positive feedback gain and $k_g = -(CA_m^{-1}B_m)^{-1}$ is a feedforward prefilter applied to the reference signal $r(t)$.

The control law for our system becomes:
$u_a(s) = -kD(s)(\hat{\eta}_l(s) - k_g r)$ with $\hat{\eta}_l$ the output of block 4. To account for the transformation of the state matrix A into A_m, the complete control input becomes: $u = u_a + u_m$ with $u_m = -k_m x(t)$. To ensure stability, the feedback gain k and the filter $D(s)$ must be carefully chosen in order to fulfill the $\mathcal{L}_1$ norm condition. The reader can refer to [14] for the detailed complete proof of stability.

C. Implementation of the Controller on the Modified AC-ROV Prototype

We wish to control the AC-ROV in depth and pitch based on the dynamics (8). For this purpose, the matrix A is converted into A_m with a chosen gain k_m fulfilling the stability requirements [14], with $A_m \in \mathbb{R}^{4\times4}$ and $B_m \in \mathbb{R}^{4\times2}$. The parameters' vector $\hat{\theta} \in \mathbb{R}^2$ is initialized to zero and represents the uncertainties on the damping coefficient and is given by: $\hat{\theta} = \left[\Delta(-D_z^*)\,,\ \Delta(-D_\vartheta^*)\right]^T$. The parameter $\sigma \in \mathbb{R}^2$ is a lumped parameter including the gravitational and buoyancy forces as well as the external disturbances $\hat{\sigma} = \left[-g_z^* + w_{d_z}^*\,,\ -g_\vartheta^* + w_{d_\vartheta}^*\right]^T$. The parameter $\omega \in \mathbb{R}^{2\times2}$ will not be adapted for this study as we have a precise knowledge of the motors' features. As expressed in equation (9), the system's outputs are z and ϑ. The control input is computed in the earth frame and should be transformed into the robot frame as: $u = K^{-1}T^{-1}J^T(u_a + u_m) \in \mathbb{R}^2$, with u_a and u_m as explained in the previous section. The gains for depth control are chosen as $\Gamma_z = 100000$ and $k_z = 0.15$ being the adaptation gain and the feedback gain respectively. For the pitch angle, the gains are $\Gamma_\vartheta = 1300$ and $k_\vartheta = 1.2$. The filtering process was ensured by the choice of $D(s) = \frac{1.4}{s}$. It is worth to be noted that the gains must ensure the $\mathcal{L}_1$ norm condition, but have to be tuned empirically since there is no systematic method to chose them.

IV. Experimental Setup

A. Modified AC-ROV experimental platform

The AC-ROV submarine (cf. Fig. 1) is an underactuated vehicle, the propulsion system of which consists of six thrusters driven by DC motors and acting on five degrees of freedom. Motors $1, 2, 3$ and 4 control simultaneously translations along x and y axes and rotation around the z axis (yaw). Motors 5 and 6 control depth and pitch. Roll is left uncontrolled but remains naturally stable thanks to the positive metacentric distance. The robot weighs 3kg and has a rectangular shape with 203mm height, 152mm length and 146mm width. For measurements purposes, our prototype is equipped with various sensors. A 6-DOF IMU (Inertial Measurement Unit) measures roll, pitch, and yaw along with their respective velocities and a pressure sensor allows depth measurement. To pre-process and transmit the sensors' data to the PC, a microcontroller board is used. Once the control law has been computed by the control PC, the control inputs are transmitted to the power stage. Then, 6 PWM modulated signals are sent to the motors of the AC-ROV through the 40-meter long tether. Fig. 3 shows a schematic view summarizing the various components of the vehicle's hardware and their interactions.

B. Conditions of the Experiments

The experiments have been performed in a $5m^3$ pool. The tether has been sufficiently unrolled to avoid inducing additional drag into the dynamics of the vehicle. The feedback gains have been tuned for the nominal conditions and kept unchanged for the other experiments despite some eventual changes in the model or its environment in order to evaluate the robustness of the proposed controller. The noisy data of depth measurement are filtered using a second order Butterworth filter. The information concerning the velocity in the z direction is estimated by an alpha-beta observer. Fig. 4 gives an overview of the whole used experimental test-bed.

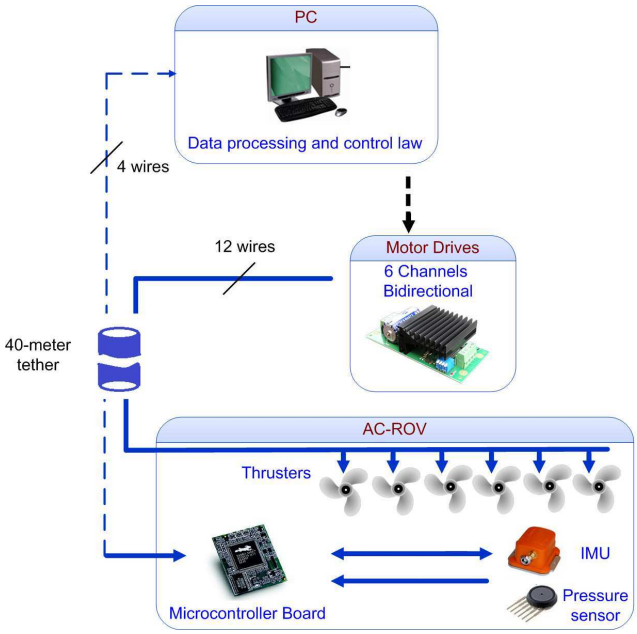

Fig. 3: Schematic view of the hardware architecture of AC-ROV prototype.

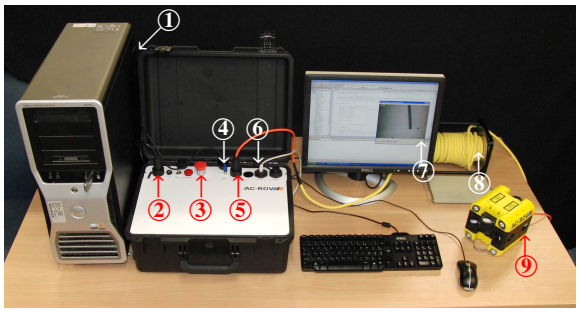

Fig. 4: View of the AC-ROV experimental test-bed: ① Control PC, ② Power input, ③ Emergency stop button, ④ Video in, ⑤ Tether plug, ⑥ Ethernet plug, ⑦ Video Capture, ⑧ Tether, ⑨ AC-ROV.

V. Real Time Experiments

A. Experimental scenarios

The experiments presented in this section result from the application of the proposed controller detailed in section 3, to the underwater vehicle testbed described in section 4. We will start by giving an overview of the different performed scenarios, then we will analyze the obtained results for each scenario. The vehicle's depth is regulated to reach 0.5m when starting from a static surface position. The pitch angle is controlled to follow a varying trajectory starting from 0° and changing to 15° at 35 seconds. The evolution of the control inputs, generated by the thrusters controlling the movements along the z axis and the pitch angle are also plotted for each scenario as well as θ and σ being respectively the estimated parameters and the disturbances pertaining to each degree of freedom.
Three experimental scenarios were performed, namely:

Scenario 1: *Control in Nominal Conditions.*
The objective of this scenario is to control depth and pitch angle of the AC-ROV without any external disturbance. The gains for each controller have been tuned to accomodate this case and were kept unchanged for the other experiments.
Scenario 2: *Robustness towards parameters'uncertainty:* Change in Buoyancy.
The model of the vehicle has been changed by the addition of a rectangular piece of polyester introducing a change of buoyancy of approximately 0.32N (which represents a +32% increase of the flottability). The objective of this scenario is to see whether the proposed controller is sufficiently robust to compensate this uncertainty and keep the performance of the controlled closed-loop system. Such a disturbance may occur for instance when the robot navigates in environments with strong salinity changes (e.g undersea fresh water spring) or when the payload of the robot is changed (e.g additional sensors).
Scenario 3: *Persistent External Disturbance Rejection:* Waves.
Waves were generated manually by periodically disturbing the surface of the pool, which created waves of approximately 15cm amplitude.

The obtained results for these three scenarios are presented and discussed in the following.

B. Scenario 1: Control in Nominal Conditions (results)

Fig. 5 displays the evolution of the controlled vehicle's depth and pitch angle. The desired depth is reached smoothly in around 40 seconds. A similar response is observed for the pitch angle, except that the convergence time is longer (65 seconds). The small initial oscillations of ϑ will be present in all the scenarios and they are caused by the differences in the starting torques (due to dry friction) of the thrusters 5 and 6. These latters reach steady state forces of -0.18N and -0.66N respectively. Their plots displayed in Fig. 5b converge to their final values with neither oscillation, nor overshoot, despite the lack of knowledge of our model parameters. The parameters vectors $\hat{\theta}$ and $\hat{\sigma}$ initialized to 0 and depicted in Fig. 5c converge to the following steady state values: $[\hat{\theta}_z \ \hat{\theta}_\vartheta]^T = [-8 \ \ -2.25]^T$ and $[\hat{\sigma}_z \ \hat{\sigma}_\vartheta]^T = [-48 \ \ -5]^T$. It can be noticed that unlike nonlinear state feedback adaptive controller the $\mathcal{L}_1$ controller ensures a fast convergence even without any a priori estimate of the unknown parameters.

C. Scenario 2: Robustness Towards Parameters Uncertainty: Change in Buoyancy (results)

Like in the previous scenario, parameters are expected to converge to new values to compensate for this change in order for the controlled degrees of freedom to be steered to their desired trajectories. The depth response (cf. Fig. 6a) converges in 40 seconds as well; it is seen to exhibit the same behavior observed in the nominal conditions (cf. Fig. 5a). The same convergence time is also conserved for the pitch angle. Although the buoyancy change has hardly no effect on the responses, interesting changes can be observed

in the control inputs and the parameters. The forces needed at steady state are -0.12N and -0.75N, and are seen to be different than the nominal scenario since more force is now required to immerse the vehicle. The parameters converge to the following values: $[\hat{\theta}_z\ \hat{\theta}_\vartheta]^T = [-8\ \ -2]^T$ and $[\hat{\sigma}_z\ \hat{\sigma}_\vartheta]^T = [-65\ \ -6]^T$. It was expected that vector $\hat{\theta}$ does not vary since it holds the parameters of damping that were kept unchanged with this modification, which only affected the buoyancy force present in vector $\hat{\sigma}$. This force has an important impact on the motion along the z axis which can be observed through the change in the parameter $\hat{\sigma}_z$ (from -48 to -65). The main interest of this scenario is to highlight the fact that due to its large adaptation gain, the convergence time of the $\mathcal{L}_1$ controller remains nearly constant even with a strong model change.

D. Scenario 3: Persistant External Disturbance Rejection: Waves (results)

The obtained results for this scenario are depicted in Fig. 7. Fig. 7a shows the system response in presence of waves. The depth is not seen to be affected by this persistant disturbance while varying oscillations of approximately 5°of amplitude around the regulated pitch angle are observed in the response of ϑ. This can be explained by the different dynamics of each degree of freedom. The translation around the z axis is less sensitive to external disturbances than the pitch angle due to the robot's inertia. Oscillations of approximately 0.07N are also observed in the control input but they are more significant in $\hat{\theta}_\vartheta$ and $\hat{\sigma}_\vartheta$ which explains the maintained oscillations of the pitch reponse. z converged to the desired depth of 0.5m in 40 seconds with $\hat{\theta}_z = -14.5$ and $\hat{\sigma}_z = -60$. The parameters damping were changed with respect to their nominal conditions and this change is reflected in the steady state value of $\hat{\theta}_z$ that was -8 in the nominal case and becomes -14.5 in presence of waves. The induced disturbances along the z axis caused by the waves are incorporated in $\hat{\sigma}_z$ that varied from -48 in the nominal conditions to -60 in this present scenario.

VI. Conclusion and Future Work

This paper deals with the problem of depth and pitch control of an underwater vehicle (a multivariable system with coupled high nonlinear dynamics). The proposed solution lies in the design and implementation of an $\mathcal{L}_1$ adaptive controller, novel in the field of underwater robotics. This controller was tested in nominal case and in other scenarios to evaluate its robustness towards parameters' uncertainties as well as its capability of rejection of external disturbances. The $\mathcal{L}_1$ adaptive controller was observed to ensure a smooth convergence to the desired trajectory in the two studied degrees of freedom and compensate for the external disturbances as well as the change in buoyancy. Our future work will include the control of the remaning degrees of freedom of the robot.

Acknowledgments

The authors would like to thank Tecnalia Foundation for its support.

References

[1] E. Roche, O. Sename, D. Simon, and S. Varrier, "A hierarchical varying sampling $\mathcal{H}_\infty$ control of an auv," in *18th IFAC world congress*, (Milano, Italy), 2011.

[2] A. Pisano and E. Usai, "Output-feedback control of an underwater vehicle prototype by higher-order sliding modes," *Automatica*, vol. 40, no. 9, pp. 1525–1531, 2004.

[3] M. Carreras, J. Yuh, and J. JBatlle, "High-Level control of autonomous robots using a behavior-based scheme and reinforcement learning," in *15th Triennial World Congress of the International Federation of Automatic Control*, (Barcelona), 2002.

[4] T. Kim and J. Yuh, "A novel neuro-fuzzy controller for autonomous underwater vehicles," in *Proceedings of the IEEE International Conference on Robotics and Automation ICRA'99*, vol. 4, pp. 2350–2355, 2001.

[5] M. Chang, W. Chang, and H. Liu, "Model-based fuzzy modeling and control for autonomous underwater vehicles in the horizontal plane," *Journal of Marine Sciences and Technology*, vol. 11, pp. 155–163, 2003.

[6] A. El-Fakdi and M. Carreras, "policy gradient based reinforcement learning for real autonomous underwater cable tracking," in *IEEE International Conference on Intelligent Robots and Systems*, (Nice, France), 2008.

[7] A. Marzbanrad, M. Eghtesad, and R. Kamali, "A robust adaptive fuzzy sliding mode controller for trajectory tracking of rovs," in *50th IEEE Conference onf Decision and Control and European Control Conference (CDC-ECC)*, (Orlando, FL), pp. 2863–2869, 2011.

[8] W. M. Bessa, M. S. Dutra, and E. Kreuzer, "Depth control of remotely operated underwater vehicles using an adaptive fuzzy sliding mode controller," *Robotics and Autonomous Systems*, vol. 5, no. 8, pp. 670–677, 2008.

[9] G. Antonelli, F. Cacciavale, S. Chiaverini, and G. Fusco, "A novel adaptive control law for Autonomous Underwater Vehicle," in *Proceedings of the IEEE International Conference on Robotics and Automation ICRA'01*, (Seoul, Korea), pp. 447–452, 2001.

[10] B. D. Anderson, "Failures of adaptive control theory and their resolution," *Communications in Information and Systems*, vol. 5, pp. 1–20, 2005.

[11] C. Rohrs, L. Valavani, M. Athans, and G. Stein, "Stability problems of adaptive control algorithms in the presence of unmodeled dynamics," (Orlando,FL), 21st Conference on Decision and Control, December 1982.

[12] Z. Zang and R. Bitmead, "Transient bounds for adaptive control systems," pp. 2724–2729, IEEE Conference on Decision and Control, 1990.

[13] K. Narendra and A. Annaswamy, "A new adaptive law for robust adaptation without persistent excitation," *IEEE Transactions on Automatic Control*, vol. 32, pp. 134–145, 1987.

[14] N. Hovakimyan and C. Cao, $\mathcal{L}_1$ *Adaptive Control Theory*. Society of Industrial and Applied Mathematics, 2010.

[15] E. Kharisov and N. Hovakimyan, "Comparison of several adaptive controllers according to their robustness metrics," (Toronto, CA), AIAA Guidance, Navigation and Control Conference, August 2010.

[16] E. Xargay, N. Hovakimyan, and C. Cao, "Benchmark problems of adaptive control revisited by $\mathcal{L}_1$ adaptive control," (Thessaloniki), pp. 31 – 36, 17th Mediterranean Conference on Control and Automation, June 2009.

[17] V. Dobrokhodov, E. Xargay, N. Hovakimyan, I. Kaminer, I. Kitsios, C. Cao, I. Gregory, and L. Valavani, "Experimental validation of $\mathcal{L}_1$ adaptive control: Rohrs' counterexample in flight," *Journal of Guidance, Control, and Dynamics,*, 2010.

[18] I. Kaminer, A. Pascoal, E. Xargay, C. Cao, and V. Dobrokhodov, "Path following for unmanned aerial vehicles using $\mathcal{L}_1$ adaptive augmentation of commercial autopilots," *Journal of Guidance, Control and Dynamics*, vol. 33, no. 2, 2010.

[19] L. Techy, C. Reddy, C. A. Woolsey, C. Cao, and N. Hovakimyan, "Nonlinear control of a novel two-link pendulum," (New York City,USA), pp. 19–24, American Control Conference, 2007.

[20] X. Fan and R. Smith, "$\mathcal{L}_1$ adaptive control of hysteresis in smart materials," (San Diego, CA), Proceedings of the SPIE Smart Structures/NDE, 15th Annual International Symposium, March 2008.

[21] T. Fossen, *Marine Control Systems:Guidance, Navigation and Control of Ships, Rigs and Underwater Vehicles*. As,Trondheim: Marine Cybernetics, 2002.

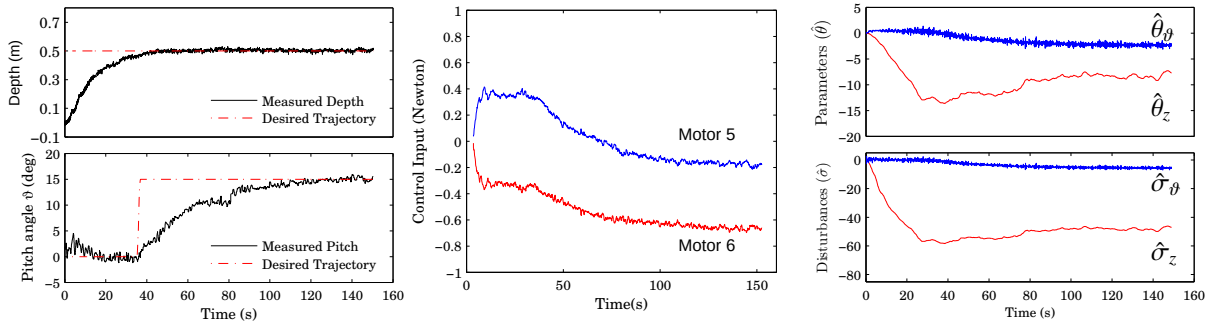

(a) Time history of the measured depth position z and pitch angle ϑ as well as their respective desired trajectories.

(b) Time history of the force exerted by the two motors controlling z and ϑ.

(c) Time history of the evolution of the parameters $\hat{\theta} = [\hat{\theta}_z \ \hat{\theta}_\vartheta]^T$ and the nonlinear terms $\hat{\sigma} = [\hat{\sigma}_z \ \hat{\sigma}_\vartheta]^T$.

Fig. 5: **Control in nominal case:** plots of (a) the system outputs (z and ϑ), (b) the control inputs, and (c) parameters $\hat{\theta}$ and $\hat{\sigma}$.

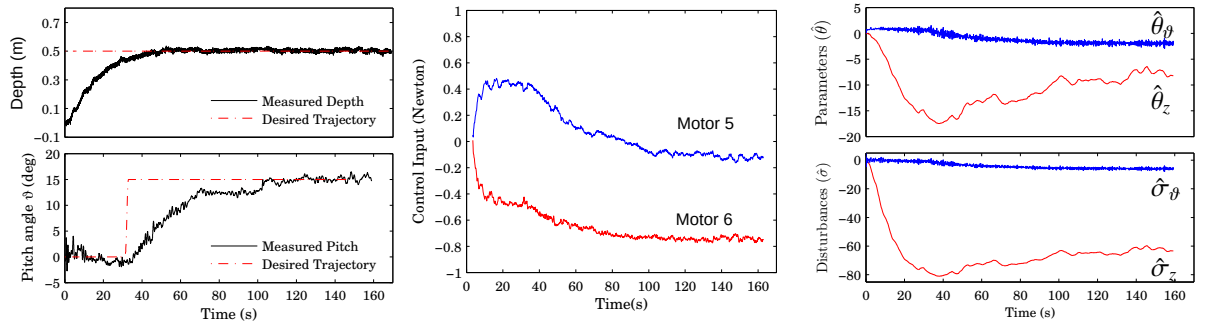

(a) Time history of the measured depth position z and pitch angle ϑ as well as their respective desired trajectories.

(b) Time history of the force exerted by the two motors controlling z and ϑ.

(c) Time history of the evolution of the parameters $\hat{\theta} = [\hat{\theta}_z \ \hat{\theta}_\vartheta]^T$ and the nonlinear terms $\hat{\sigma} = [\hat{\sigma}_z \ \hat{\sigma}_\vartheta]^T$.

Fig. 6: **Robustness towards parameters uncertainty:** change in buoyancy: plots of (a) the system outputs (z anf ϑ) are very similar to the nominal case. The change of buoyancy is observed through the plots of the control inputs (b) and the controlled parameters $\hat{\theta}$ and $\hat{\sigma}$ (c) .

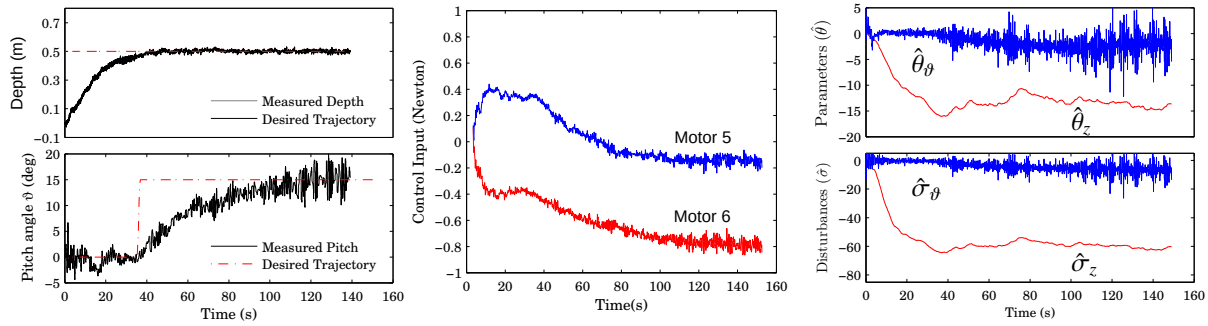

(a) Time history of the measured depth position z and pitch angle ϑ as well as their respective desired trajectories.

(b) Time history of the force exerted by the two motors controlling z and ϑ.

(c) Time history of the evolution of the parameters $\hat{\theta} = [\hat{\theta}_z \ \hat{\theta}_\vartheta]^T$ and the nonlinear terms $\hat{\sigma} = [\hat{\sigma}_z \ \hat{\sigma}_\vartheta]^T$.

Fig. 7: **Persistant external disturbances rejection (waves):** only the pitch angle was affected by the waves while the depth response has the same behavior as in the nominal case (a). The introduction of this external disturbance is reflected in the oscillations of the control inputs (b) and the controlled parameters (c).